



Trans. Nonferrous Met. Soc. China 33(2023) 3661-3672

Transactions of Nonferrous Metals Society of China

www.tnmsc.cn



Preparation of ultrafine-grained Mg-Mn-Ce alloy with high ductility and energy absorption by coupling extrusion and forging

Yu-xiu ZHANG¹, Zhi-rou ZHANG¹, Chun-yu WANG¹, Hong-hui KANG¹, Hiromi NAGAUMI², Xu-yue YANG¹

- 1. School of Materials Science and Engineering, Central South University, Changsha 410083, China;
 - 2. School of Iron and Steel, Soochow University, Suzhou 215100, China

Received 27 May 2022; accepted 10 November 2022

Abstract: An ultrafine-grained (UFGed) Mg-0.9Mn-0.5Ce (wt.%) alloy with high compressive ductility and energy absorption was developed using a low-temperature deformation method of coupling extrusion and forging. Specifically, the alloy was extruded at 150 °C with an extrusion ratio of 12:1, followed by forging at 200 °C to a true strain of 1.2 along the extrusion direction. The microstructure and plastic mechanism were uncovered using optical microscopy, scanning electron microscopy, electron backscatter diffraction and transmission electron microscopy. The microstructure was found to consist of ultrafine dynamically recrystallized (DRXed) grains and fragmented unDRXed grains, exhibiting an average grain size of 1.9 μm after low-temperature extrusion. After forging, new UFGs were gradually generated, a uniform UFGed microstructure with an average grain size of 2.7 μm was obtained, and the texture intensity was decreased as well. The homogenous UFGs and basal slip collaboratively contributed to better comprehensive performance of the UFGed alloy, such as a high compressive ductility of 45.0% and a high energy absorption of 122.72 MJ/m³.

Key words: Mg-Mn-Ce alloy; ultrafine grain; ductility; energy absorption

1 Introduction

The demand for lightweight materials in the automobile industry has led to the utilization of magnesium (Mg) alloys because of their advantages of low density and high specific strength [1–3]. However, the dilemma of low absolute strength and ductility severely restricts the practical applications of Mg alloys. Especially under compressive loading, as encountered in a minor collision, the low energy absorption cannot ensure structural stability and security, which is closely related to the combination of strength and ductility [4,5]. To achieve high energy absorption, the priority is to simultaneously improve ductility and ensure adequate strength.

In terms of improving the mechanical properties, it has been frequently reported that the

addition of rare earth (RE) elements into Mg alloys can lead to unexpected achievements because RE elements exhibit outstanding solution strengthening, precipitation strengthening and texture weakening effects [3,6-10]. However, a considerably high content of RE elements is usually needed for realizing the desired mechanical properties. In consideration of the high price of RE elements, the price of associated products is definitely increased. In addition, although highly concentrated Mg-RE alloys show impressive strength they usually exhibit limited ductility [10-12]. An alternative method for increasing the mechanical properties of Mg alloys is to considerably diminish the grain size and modify the texture by using severe plastic deformation (SPD) processes, such as equalchannel angular pressing (ECAP), differential speed rolling (DSR) and multi-directional forging (MDF) [13–15]. Nevertheless, fine-grained Mg alloys obtained by SPD usually show high strength but limited ductility because enormous defects, including high density dislocations, twins, stacking faults or even micro-crack, can lead to strong work hardening and hinder further deformation [15,16]. Thus, a valid and practical process technology is urgently needed to develop Mg alloys with high ductility and energy absorption.

Recently, some researchers have explored the method of low-temperature extrusion to develop high-performance Mg alloys [17-19]. In comparison to SPD methods, low-temperature extrusion is an inexpensive and prolific method for industrial production. However, such a method inevitably leads to a decreased volume fraction of dynamic recrystallized (DRXed) grains due to the extremely low temperature, which is contrary to the acquisition of a homogenous ultrafine-grained (UFGed) microstructure and the improvement of ductility [20]. Although the volume fraction of DRXed grains can be enhanced by increasing the extrusion temperature and extrusion ratio or decreasing the extrusion speed, such a method has been proven to be less reliable for the improvement of the ductility [20-22]. Subsequent annealing treatment can also be used to homogenize the extruded microstructure but at the expense of decreased strength, and the ductility is limitedly improved because grains can easily grow, especially for low-alloyed Mg alloys [23]. For the above reasons, for low-temperature extruded Mg alloys, a deeper and more reasonable process is needed to increase the volume fraction of UFGs and improve the ductility.

In this work, a two-step deformation method was scrupulously designed and successfully employed for a dilute Mg-Mn-Ce alloy to obtain high compressive ductility and energy absorption. Specifically, the alloy was first subjected to extrusion at 150 °C, followed by forging at 200 °C. It has been reported that Mn exhibits extraordinary potential to improve the formability of Mg alloys, and Ce has an outstanding inhibited effect on the growth of DRXed grains due to pinning of grain boundaries [9,24]. Combined with the low-temperature deformation method, a low-alloyed UFGed Mg-Mn-Ce alloy with excellent compressive ductility and energy absorption was successfully fabricated. The corresponding

microstructure and plastic mechanism were uncovered. Studies on the low-alloyed Mg alloys show promising potential for resource savings and environmental protection. It is believed that such an investigation on the development of dilute Mg–Mn–Ce alloys with high ductility and energy absorption can expand the practical applications of Mg alloys.

2 Experimental

An alloy ingot with the nominal composition of Mg-0.9Mn-0.5Ce (wt.%) was prepared from high purity magnesium (99.9 wt.%), Mg-6.4Mn (wt.%) and Mg-30Ce (wt.%) master alloys at 720 °C under a SF₆ and CO₂ protective atmosphere. The cast ingot was subjected to homogeneous treatment at 500 °C for 24 h, followed by hot extrusion. An extruded rod with a diameter of 15 mm was obtained at 150 °C with an extrusion ratio of 12:1 and an extrusion speed of 0.1 mm/s. Forging samples with a height of 18 mm along the extrusion direction (ED) and a diameter of 12 mm along the transverse direction (TD) were machined from the extruded rod. Forging was conducted at 200 °C with a strain rate of 3.0×10^{-3} s⁻¹ to a true strain of 1.2 along the ED. Graphite powder was used to reduce the friction between the samples and compression molds. To ensure uniform heating, the samples and molds were preserved at the forging temperature for 30 min. The samples were immediately quenched in water after forging to reserve the microstructure. Compressive samples with a height of 5 mm and a diameter of 4 mm were machined with the loading direction parallel to the ED. Compressive tests were conducted at room temperature with a strain rate of 3.0×10^{-3} s⁻¹ using an Instron-type mechanical testing machine. For brevity, the as-homogenized sample was abbreviated as the AH sample, the as-extruded sample was abbreviated as the AE sample and the as-forged sample was abbreviated as the AF sample.

The microstructures were observed using optical microscopy (OM), scanning electron microscopy (SEM), electron backscatter diffraction (EBSD) and transmission electron microscopy (TEM) apparatus, respectively. For OM observation, the samples were mechanically ground and then etched in acetic picral (2.1 g picric acid + 5 mL water + 5 mL acetic acid + 35 mL ethanol). For SEM and EBSD

observations, the samples were mechanically ground and then electropolished in a mixed solution of nitric acid and ethanol with a volume ratio of 1:10. For TEM observation, the samples were punched into disks with a diameter of 3 mm, mechanically ground to a thickness of $\sim 80 \, \mu m$, and finally perforated by the ion-beam thinning method.

3 Results and discussion

3.1 Compressive properties

Figure 1 presents the engineering stress-strain measured for all samples during compressive tests, and the mechanical properties are summarized in Table 1. As observed, the mechanical properties of the AH sample are greatly improved after low-temperature extrusion. The yield strength (YS), ultimate compressive strength (UCS) and fracture elongation (FE) are 113 MPa, 128 MPa and 13.3% for the AH sample and 205 MPa, 289 MPa and 20.4% for the AE sample, respectively. After forging, the UCS and FE are further improved, although the YS is slightly decreased, leading to a good balance of strength and ductility. Specifically, the AF sample shows a YS, UCS and FE of 180 MPa, 356 MPa and 45.0%, respectively, indicating that the UCS and FE are improved by ~23\% and ~127\%, respectively, compared with that for the AE sample. Moreover, the energy absorption for all samples is also listed in Table 1. In general, the energy absorption per unit volume is calculated as the area enclosed by the stress-strain curve against fracture, meaning that a good balance of strength and ductility always leads to high energy absorption before fracture. The energy absorption values of the AH and AE samples are determined to be 15.05 and 45.38 MJ/m³, respectively. After forging, a pronounced energy absorption of 122.72 MJ/m³ is obtained because of the excellent ductility, which is improved by 170.4% compared with that for the AE sample.

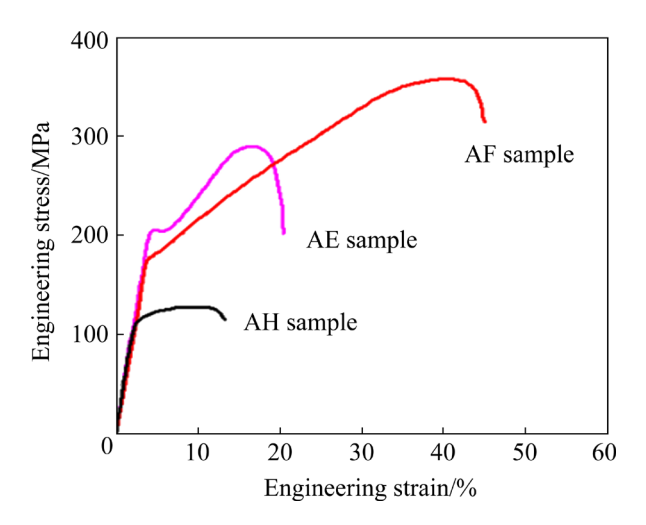


Fig. 1 Engineering stress-strain curves of AH, AE and AF samples

Table 1 YS, UCS, FE and energy absorption of AH, AE and AF samples measured by compressive tests

Sample	YS/	UCS/	FE/	Energy absorption/
	MPa	MPa	%	$(MJ \cdot m^{-3})$
AH	113	128	13.3	15.05
AE	205	289	20.4	45.38
AF	180	356	45.0	122.72

3.2 Microstructures before compressive tests

Figure 2 shows the typical OM images obtained for all samples before the compressive tests. For the AH sample, the grain size is considerably decreased after the low-temperature extrusion. The ultrafine DRXed grains and fragmentized unDRXed grains are simultaneously obtained in the AE sample (see Figs. 2(a) and (b)). Although low-temperature extrusion is able to inhibit the growth of DRXed grains, the number of DRX nucleation sites is definitely decreased, which leads to an incomplete recrystallization microstructure. After subsequent forging, newly DRXed grains evolve, which originate from the original

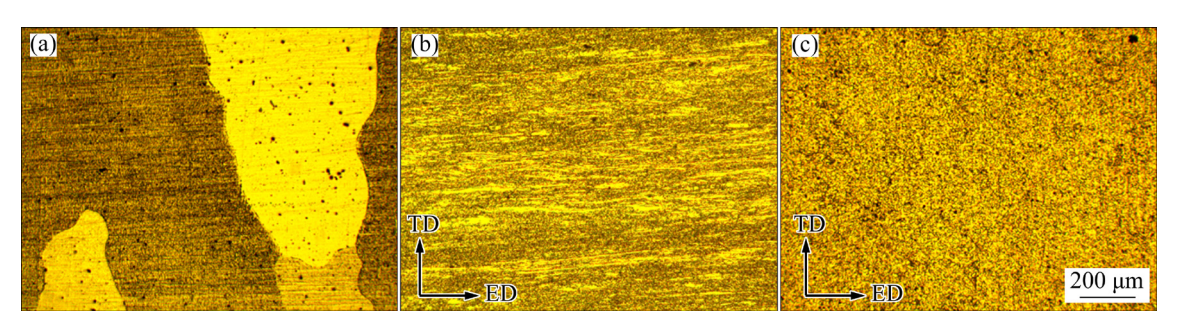


Fig. 2 Typical OM images of AH (a), AE (b) and AF (c) samples

unDRXed grains, and a fully DRXed microstructure with uniform UFGs is formed in the AF sample (see Fig. 2(c)).

As shown in Fig. 3, the microstructures of the AE and AF samples can be further explored by EBSD. According to the inverse pole figure (IPF), the AE sample clearly shows the combination of ultrafine DRXed grains and fragmented unDRXed grains (see Fig. 3(a)), while the AF sample exhibits an extremely homogeneous UFGed microstructure (see Fig. 3(b)). The corresponding {0001} pole figure shows that a typical extruded texture with basal planes oriented parallel to the ED is formed in

the AE sample (see Fig. 3(c)). Unlikely, a relatively weak basal texture with basal planes tilted towards the ED is formed after subsequent forging because the volume fraction of UFGs is increased (see Fig. 3(d)) [10]. The grain size distribution is shown in Figs. 3(e) and (f), and the average grain sizes in AE and AF samples are calculated to be 1.9 and 2.7 µm, respectively, based on EBSD measurements. Namely, the subsequent forging can acquire a homogenous microstructure at the expense of a slight increment in the average grain size, which is a critical consideration for realizing enhanced ductility and energy absorption.

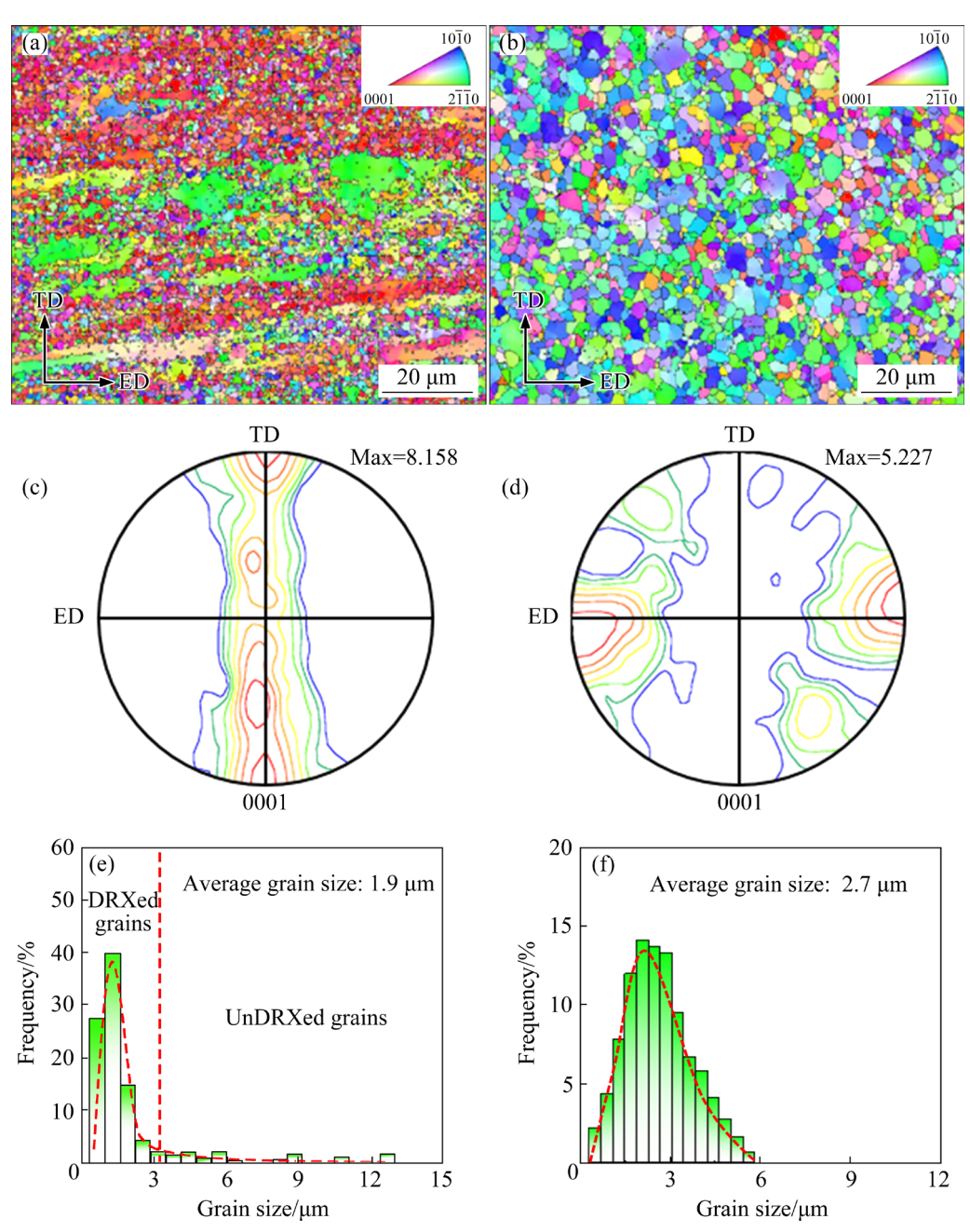


Fig. 3 Typical IPFs (a, b), corresponding {0001} pole figures (c, d), and grain size distribution (e, f) before compressive tests: (a, c, e) AE sample; (b, d, f) AF sample

It is well known that basal slip commonly plays an important role in deformability and is usually regarded as the primary consideration for the ductility in Mg alloys at room temperature because of the extremely low critical resolved shear stress (CRSS) [25]. The Schmid factor (SF) distribution maps for the basal slip in AE and AF samples are presented in Fig. 4. Because of the weak basal texture, a majority of grains are found to show a strong tendency for basal slip in the AF sample, and the average SF value (0.35) is much higher than that in the AE sample (0.19). Apparently, basal slip can be frequently activated and expectedly leads to excellent ductility in the AF sample.

During forging at 200 °C, dislocation recovery and dynamic recrystallization are promoted. The density of residual dislocations in the AF sample is speculated to be lower than that in the AE sample. Figures 5(a) and (b) present the kernel average misorientation (KAM) maps obtained before compressive tests to compare the densities of residual dislocations in the AE and AF samples, respectively [26]. Obviously, the dislocation density in the AE sample is higher, and the stress accumulation derived from the residual dislocations is mainly concentrated in the unDRXed grains. This

is probably caused by the high-density dislocations that accommodate the local lattice strains in the unDRXed grains [27-29]. In contrast, low density dislocations and homogenous stress distributions are observed in the AF sample, resulting from the energy consumption by dynamic recrystallization and dynamic recovery during forging. In addition, TEM bright field measurements are used to intuitively observe residual dislocations. As shown in Fig. 5(c), high-density dislocations are precisely observed in the unDRXed grains of the AE sample, while the dislocation traces are barely found in the DRXed grains (see Fig. 5(e)). Nevertheless, the homogenous contrast means that the AF sample is composed of deformed UFGs (marked by the red lines), and the newly formed DRXed grains (marked by the blue lines) have low-density dislocations (see Fig. 5(d)).

In general, most residual dislocations are considered geometrically necessary dislocations (GNDs) for accommodating local strain, which can be estimated from the following approach [26,30,31]:

$$\rho_{\text{GND}} = 2\theta/(ub) \tag{1}$$

where ρ_{GND} is the residual dislocation density; θ is the misorientation angle; u is the unit length of a circuit around a specific point of interest, which is

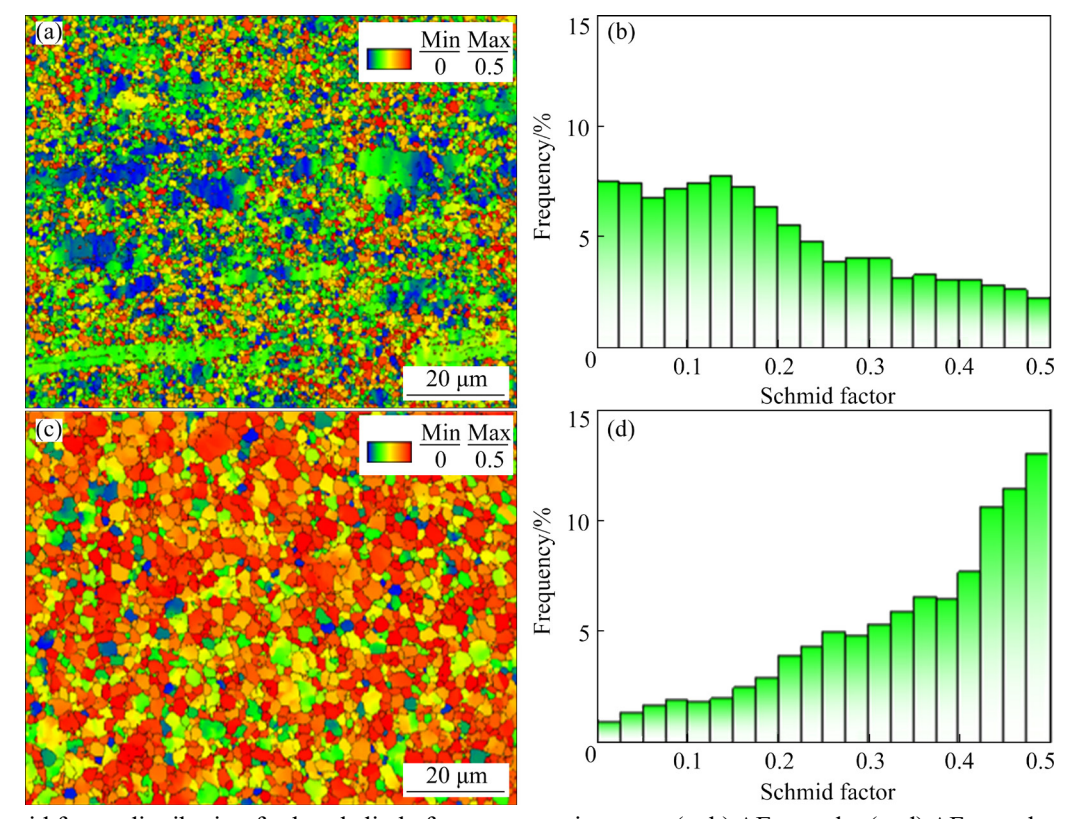


Fig. 4 Schmid factor distribution for basal slip before compressive tests: (a, b) AE sample; (c, d) AF sample

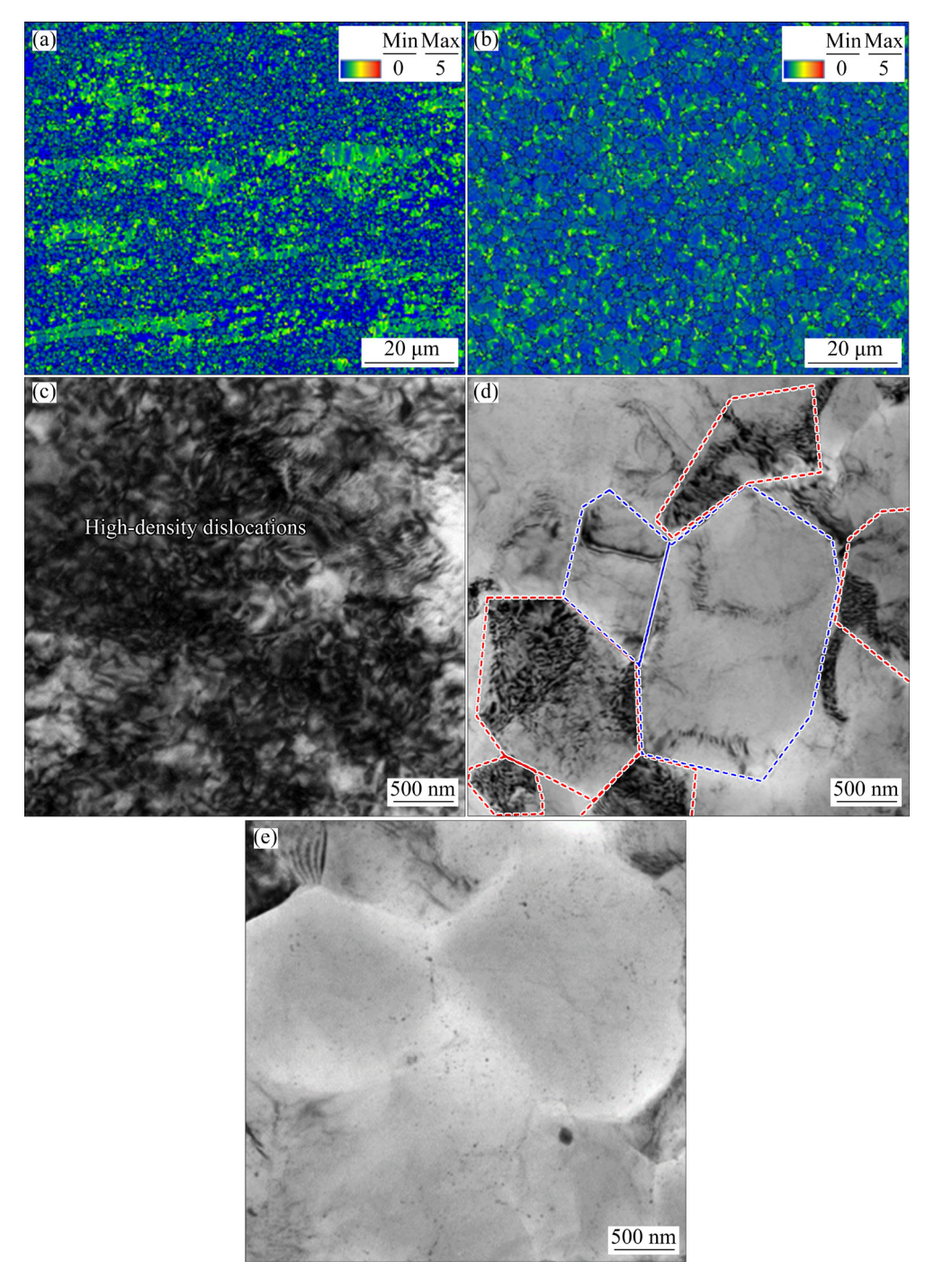


Fig. 5 Typical KAM maps (a, b) and TEM bright field images (c, d, e) before compressive tests: (a, c, e) AE sample; (b, d) AF sample

equal to twice the step size $(0.2 \,\mu\text{m})$ used in EBSD acquisition; b is the magnitude of the Burgers vector $(0.32 \,\text{nm})$. According to the θ values quantified using KAM maps $(0.42^{\circ} \,\text{and}\, 0.35^{\circ})$, the densities of residual dislocations in AE and AF samples are estimated to be $\sim 6.56 \times 10^{15}$ and $\sim 5.47 \times 10^{15} \,\text{m}^{-2}$, respectively. High-density dislocations inevitably induce a strong work

hardening effect, leading to a higher YS in the AE sample than that in the AF sample. Meanwhile, dislocations are known to have a higher strain energy than defect-free matrix regions because they lead to local distortion of the crystal lattice from the ideal regularity [27–29]; thus, the strain energy induced by high-density dislocations can drive dynamic recrystallization and ensure successful

forging at low temperatures (200 °C). Consequently, a homogenous UFGed microstructure is perfectly achieved in the AF sample.

3.3 Plastic mechanisms

Figure 6 presents the microstructures in the AE and AF samples after compression to a plastic

strain of 10% to uncover the plastic mechanisms during compressive tests. For the AE sample, deformation twins are observed in the unDRXed grains (marked by the black arrows in Fig. 6(a)), while deformation twins are barely observed in the ultrafine DRXed grains. These deformation twins are formed during the compressive test because the

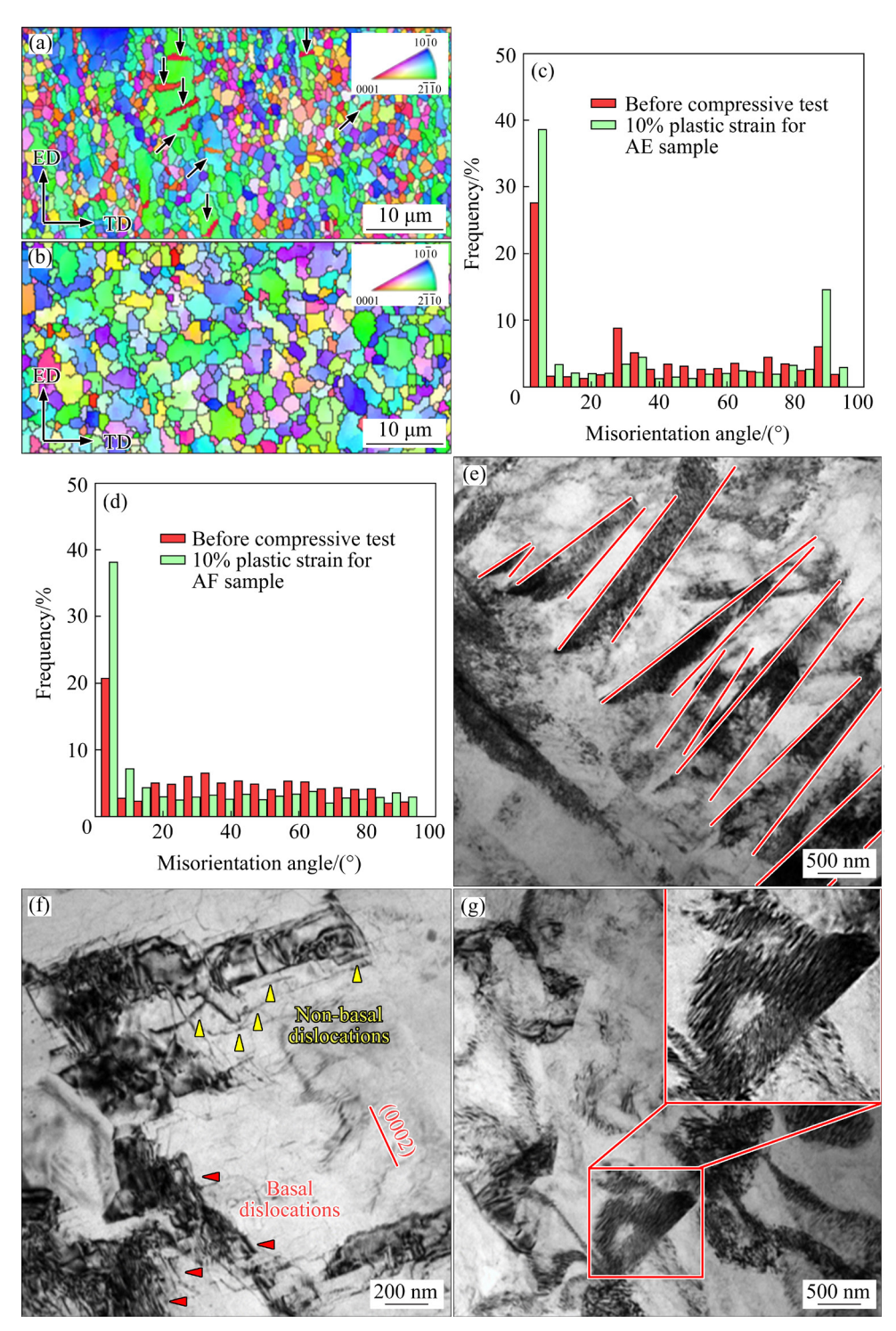


Fig. 6 Typical IPFs (a, b), misorientation angle distribution (c, d), and TEM bright field images (e, f, g) of samples after being compressed to plastic strain of 10%: (a, c, e, f) AE sample; (b, d, g) AF sample (The incident beam directions in (e) and (f) are both $B=[2\overline{110}]$)

frequency of the misorientation angle around 86° is clearly increased compared with that before the compressive test (see Fig. 6(c)). The compressive curve exhibits a concave-up shape in the early stage, which also proves the formation of $\{10\overline{12}\}$ twins during the compressive test [32]. In addition, the frequency of low-angle grain boundaries is also increased after deformation, resulting from the increased dislocations. Furthermore, the TEM bright field image shows that deformation twins are oriented parallel to each other in the unDRXed grains. High-density dislocations are concentrated in the twins, which can give rise to work hardening and hinder further deformation (see Fig. 6(e)). The suitable grain orientation and heavy back stress induced by high-density dislocations easily trigger these deformation twins in the unDRXed grains. However, the energy of twin interfaces is known to be significantly high in Mg alloys, which can lead to increased difficulty for twin nucleation with decreasing grain size [33]. In addition, the CRSS for twinning also increases with decreasing grain size [34]. Therefore, the plastic deformation mainly occurs via dislocation slip rather than twinning in the UFGs (see Fig. 6(f)). Under the incident beam direction $B = \begin{bmatrix} 2\overline{1}\overline{1}0 \end{bmatrix}$, the basal plane can be viewed as an edge or a line because it is oriented parallel to the incident beam direction. For this reason, the dislocations are determined to be basal dislocations when they are oriented parallel to the basal plane trace. Otherwise, they are identified as non-basal dislocations [3]. Therefore, basal dislocations and non-basal dislocations are determined by identifying simultaneously geometric relationship between the dislocation lines and the trace of the basal plane (the red line).

For the AF sample, deformation twins are barely observed in all grains, indicating that twinning is also ruthlessly restricted by homogeneous UFGs and inappropriate grain orientation (see Fig. 6(b)). The misorientation angle distribution map further verifies that twinning is restricted because the frequency of the ~86° misorientation angle is barely observed to change after the compressive test (see Fig. 6(d)). Instead, many short dislocation lines with parallel arrangements are expressly observed in every individual grain, indicating that basal dislocations are massively activated during deformation because the SF for the

basal slip is very high (see the enlarged image in Fig. 6(g)). As a result, the deformation mechanisms are selectively activated in the AE sample, including twinning in the unDRXed grains and dislocation slip in the ultrafine DRXed grains. In contrast, basal slip invariably dominates the plastic deformation of all UFGs in the AF sample.

Figure 7(a) shows the entity images for visually observing the difference in deformability between the AE and AF samples, in which A represents the sample before the compressive test, while B and C represent the AE and AF samples after compression for the fracture, respectively. Compared with the AE sample, a more prominent deformability is realized in the AF sample. The wrinkled and uneven surface shows that high energy absorption is explicitly tangible in the AF sample. In addition, it simultaneously indicates that homogeneous UFGs can accommodate plastic strain via grain boundary sliding (GBS), which contributes to high ductility in the AF sample. Room-temperature GBS behavior grained Mg alloys has been reported in many studies [24,35-38]. SOMEKAWA et al [35] reported that GBS contributed to the high roomtemperature tensile ductility of ~100% in an UFGed Mg-Mn-Zr alloy due to the segregation of Mn at grain boundaries, promoting GBS during deformation. Thus, GBS can work to highlight the ductility and energy absorption of dilute Mg-Mn-Ce alloys with homogeneous UFGed microstructures in this work. Moreover, the fracture morphologies of the AE and AF samples after rupture are shown in Figs. 7(b) and (c), respectively. For the AE sample, an obvious brittle fracture mode is determined because the fracture surface is extremely smooth and only a few plastic deformation traces are shown in Fig. 7(b). In other words, the crack can propagate rapidly during deformation, resulting in low ductility. For the AF sample, striations and dimples are evidently observed, which belong to the traces of dislocation slip, indicating a ductile fracture mode [39] (see Fig. 7(c)). These striations and dimples strongly contribute to the high ductility of the AF sample. UFGs are able to absorb considerable strain energy and ensure weak strain incompatibility, leading to a uniform strain distribution between different grains. In such cases, the possibility for crack nucleation

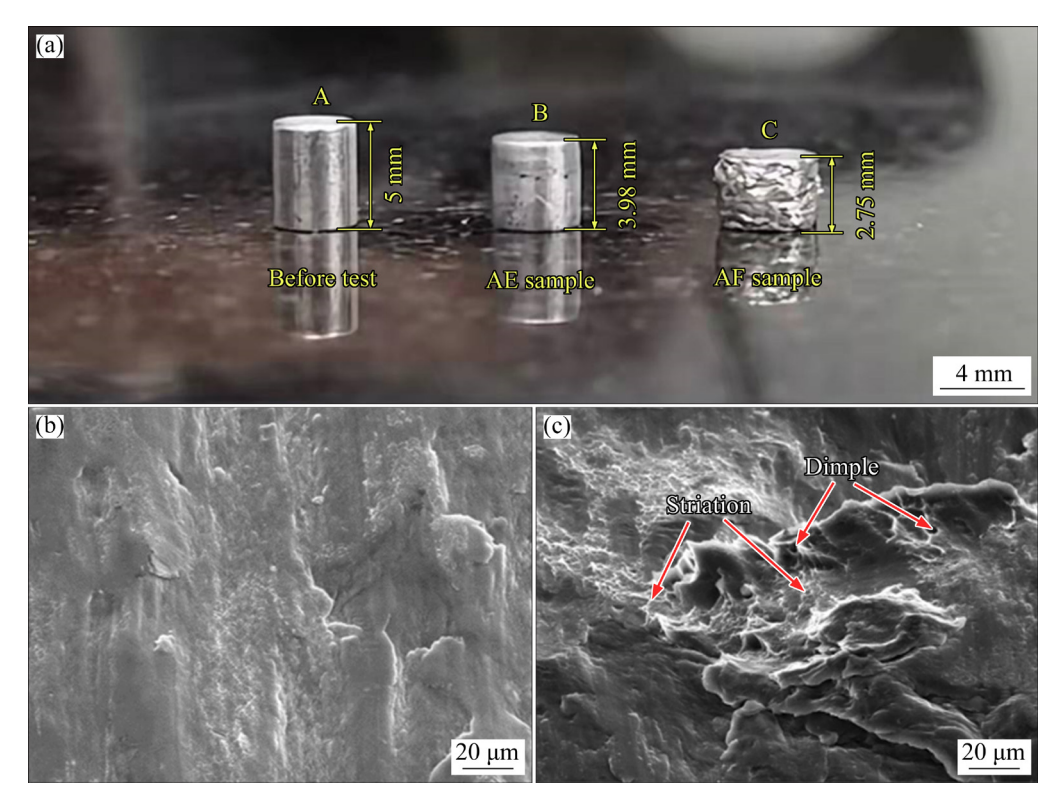


Fig. 7 Entity images before and after compressive tests (a) and typical SEM images showing fracture morphology after rupture of AE (b) and AF (c) samples

induced by stress concentration is low. Thus, the AF sample is expected to show high ductility and energy absorption before fracture. Although the average grain size of the AE sample is smaller than that of the AF sample, the heterogeneous microstructure is strongly against continuous plastic deformation. Different deformation mechanisms (twinning in the unDRXed grains and dislocation slip in the ultrafine DRXed grains) tend to induce heavy strain incompatibility between ultrafine DRXed grains and fragmented unDRXed grains during deformation, which ruthlessly restricts the comfortable deformation in the AE sample. A uniform UFGed microstructure is pragmatically understood to be the key for the fulfillment of high ductility and energy absorption, which is successfully obtained in the AF sample.

Using a low-temperature deformation method, a homogenous UFGed Mg-0.9Mn-0.5Ce alloy with excellent ductility and energy absorption is developed, as expected. It is necessary to compare the ductility and energy absorption of this alloy with those of the reported UFGed Mg alloys [40-47]. As shown in Fig. 8, under the condition of an adequate compressive strength ranging from 300 to

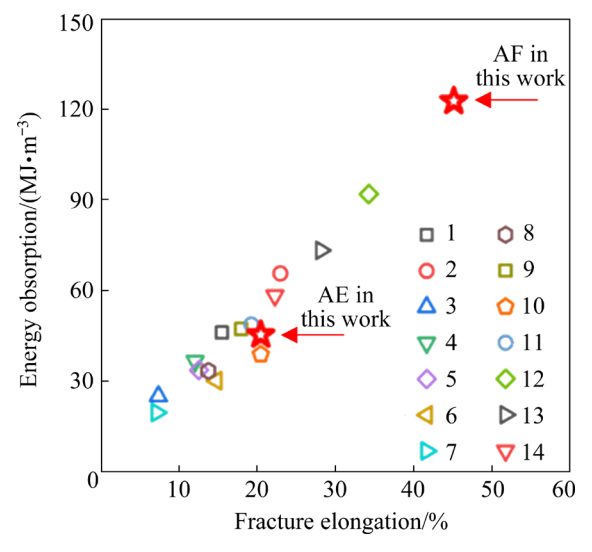


Fig. 8 Energy absorption of some UFGed Mg alloys with ultimate compressive strength ranging from 300 to 400 MPa in references in comparison to AE and AF samples in this work (1–Mg–6.63Zn–0.56Zr [40]; 2–Mg–5.25Zn–0.6Ca [41]; 3–Mg–5.1Zn–0.18Zr [42]; 4–Mg–5.1Zn–0.18Zr [42]; 5–Mg–8.8Al–0.47Zn [43]; 6–Mg–3Zn–1Al [44]; 7–Mg–5.3Zn–0.6Ca [45]; 8–Mg–2.1Mn–0.7Ce [46]; 9–Mg–2.1Mn–0.7Ce [46]; 10–Mg–2.1Mn–0.7Ce [46]; 11–Mg–2.1Mn–0.7Ce [46]; 12–Mg–2Gd–0.5Mn [47]; 13–Mg–2Gd–1.0Mn [47]; 14–Mg–2Gd–1.5Mn [47])

400 MPa, the ductility of the AF sample is greatly enhanced. In such cases, the energy absorption is profoundly higher than that of the highly alloyed Mg alloys despite low alloying. By virtue of a reasonable proceeding method, low-alloyed Mg alloys with excellent energy absorption can also be developed, which is beneficial to maintaining the advantage of lightweight and low cost products. Such an investigation can positively enrich the design process for Mg alloys with high ductility and energy absorption and expand the pragmatic applications of Mg alloys in passive safety regions.

4 Conclusions

- (1) The microstructure of the as-extruded sample consists of ultrafine DRXed grains and fragmented unDRXed grains, exhibiting an average grain size of 1.9 μ m. After forging, new UFGs are formed, a uniform UFG microstructure with an average grain size of 2.7 μ m is obtained, and the texture intensity is also decreased.
- (2) The mechanical properties of the Mg-0.9Mn-0.5Ce alloy are greatly improved after low-temperature deformation. The YS, UCS and FE are 205 MPa, 289 MPa and 20.4% for the AE sample and 180 MPa, 356 MPa and 45.0% for the AF sample, respectively.
- (3) The homogenous UFGs and basal slip contribute to the good balance of strength and ductility after two-step deformation, resulting in an impressive energy absorption of 122.72 MJ/m³.

Acknowledgments

The authors gratefully acknowledge the financial support from the National Key Research and Development Program of China (No. 2022YFE0109600, 2021YFB3701100), and the National Natural Science Foundation of China (No. 52071344, 52150710544).

References

- [1] CHAO Hong-ying, SUN Hong-fei, WANG Er-de. Working hardening behaviors of severely cold deformed and fine-grained AZ31 Mg alloys at room temperature [J]. Transactions of Nonferrous Metals Society of China, 2011, 21(Suppl.): 235–241.
- [2] ZHANG Bao-hong, ZHANG Zhi-min. Influence of homogenizing on mechanical properties of as-cast AZ31 magnesium alloy [J]. Transactions of Nonferrous Metals

- Society of China, 2010, 20(Suppl.): 439-443.
- [3] ZHANG Yu-xiu, HUO Qing-huan, ZHANG Zhi-rou, XIAO Zhen-yu, WANG Chun-yu, HASHIMOTO A, YANG Xu-yue. Effects of yttrium content on the three-dimensional compressive creep anisotropy of Mg-Y alloys [J]. Metallurgical and Materials Transactions A, 2021, 52: 3910-3930.
- [4] SHARAHI H J, POURANVARI M, MOVAHEDI M. Strengthening and ductilization mechanisms of friction stir processed cast Mg-Al-Zn alloy [J]. Materials Science and Engineering A, 2020, 781: 139249.
- [5] PENG Si-yuan, MOORAJ S, FENG Rui, LIU Liang, REN Jie, LIU Yan-fang, KONG Fan-yue, XIAO Zhi-yu, ZHU Cheng, LIAW P K, CHEN Wen. Additive manufacturing of three-dimensional (3D)-architected CoCrFeNiMn highentropy alloy with great energy absorption [J]. Scripta Materialia, 2021, 190: 46–51.
- [6] DING Zhi-bing, ZHAO Yu-hong, LU Ruo-peng, YUAN Mei-ni, WANG Zhi-jun, LI Hui-jun, HOU Hua. Effect of Zn addition on microstructure and mechanical properties of cast Mg-Gd-Y-Zr alloys [J]. Transactions of Nonferrous Metals Society of China, 2019, 29: 722-734.
- [7] HAGIHARA K, KINOSHITA A, SUGINO Y, YAMASAKI M, KAWAMURA Y, YASUDA H Y, UMAKOSHI Y. Effect of long-period stacking ordered phase on mechanical properties of Mg₉₇Zn₁Y₂ extruded alloy [J]. Acta Materialia, 2010, 58: 6282–6293.
- [8] HIDALGO-MANRIQUE P, ROBSON J D, PÉREZ-PRADO M T. Precipitation strengthening and reversed yield stress asymmetry in Mg alloys containing rare-earth elements: A quantitative study [J]. Acta Materialia, 2017, 124: 456–467.
- [9] SABAT R K, BRAHME A P, MISHRA R K, INAL K A, SUWAS S. Ductility enhancement in Mg-0.2%Ce alloys [J]. Acta Materialia, 2018, 161: 246-257.
- [10] ZHANG Zhi-rou, HUO Qing-huan, XIAO Zhen-yu, ZHANG Yu-xiu, HASHIMOTO A, YANG Xu-yue. Optimizing the mechanical properties of a Mg-Y-Nd-Zn-Zr alloy via interrupted compression with an intermediate annealing [J]. Materials Science and Engineering A, 2021, 812: 141102.
- [11] JIA Lin-yue, DU Wen-bo, WANG Zhao-hui, LIU Ke, LI Shu-bo, YU Zi-jian. Dual phases strengthening behavior of Mg-10Gd-1Er-1Zn-0.6Zr alloy [J]. Transactions of Nonferrous Metals Society of China, 2020, 30: 635-646.
- [12] ZHENG Jie, CHEN Zhe, YAN Zhao-ming, ZHANG Zhi-min, WANG Qiang, XUE Yong. Preparation of ultra-high strength Mg-Gd-Y-Zn-Zr alloy by pre-ageing treatment prior to extrusion [J]. Journal of Alloys and Compounds, 2022, 894: 162490.
- [13] BISWAS S, SINGH DHINWAL S, SUWAS S. Room-temperature equal channel angular extrusion of pure magnesium [J]. Acta Materialia, 2010, 58: 3247–3261.
- [14] LUO Dan, WANG Hui-yuan, ZHAO Li-guo, WANG Cheng, LIU Guo-jun, LIU Yan, JIANG Qi-chuan. Effect of differential speed rolling on the room and elevated temperature tensile properties of rolled AZ31 Mg alloy sheets [J]. Materials Characterization, 2017, 124: 223–228.
- [15] YANG Xu-yue, MIURA H, SAKAI T K. Structural development at severely high strain in AZ31 magnesium

- alloy processed by cold forging and subsequent annealing [J]. Materials & Design, 2013, 44: 573–579.
- [16] HUANG He, LIU Huan, WANG Ce, SUN Jia-peng, BAI Jing, XUE Feng, JIANG Jing-hua, MA Ai-bin. Potential of multi-pass ECAP on improving the mechanical properties of a high-calcium-content Mg-Al-Ca-Mn alloy [J]. Journal of Magnesium and Alloys, 2019, 7: 617-627.
- [17] YU Hui, PARK Sung-hyuk, YOU Bong-sun. Development of extraordinary high-strength Mg-8Al-0.5Zn alloy via a low temperature and slow speed extrusion [J]. Materials Science and Engineering A, 2014, 610: 445-449.
- [18] HU Ke, LI Chun-yu, XU Guo-jun, GUO Rui-zhen, LE Qi-chi, LIAO Qi-yu. Effect of extrusion temperature on the microstructure and mechanical properties of low Zn containing wrought Mg alloy micro-alloying with Mn and La-rich misch metal [J]. Materials Science and Engineering A, 2019, 742: 692–703.
- [19] NIU Yan-xia, SONG Ze-tian, LE Qi-chi, HOU Jian, NING Fang-kun. Excellent mechanical properties obtained by low temperature extrusion based on Mg-2Zn-1Al alloy [J]. Journal of Alloys and Compounds, 2019, 801: 415-427.
- [20] GÄRTNEROVÁ V, SINGH A, JÄGER A, MUKAI T. Deformation behavior of ultra-fine-grained Mg-0.3at.%Al alloy in compression [J]. Journal of Alloys and Compounds, 2017, 726: 651-657.
- [21] GU Guang-lin, KE Xiang-nan, HU Fa-ping, ZHAO Shu-jie, WEI Guo-bin, YANG Yan, PENG Xiao-dong, XIE Weidong. Fine-grained Mg-1Mn-0.5Al-0.5Ca-0.5Zn alloy with high strength and good ductility fabricated by conventional extrusion [J]. Transactions of Nonferrous Metals Society of China, 2022, 32: 483-492.
- [22] XIAO Lei, YANG Guang-yu, PEI Ri-sheng, ZHEN Zhi-li, JIE Wan-qi. Effects of extrusion ratio and subsequent heat treatment on the tension-compression yield asymmetry of Mg-4.58Zn-2.6Gd-0.18Zr alloys [J]. Materials Science and Engineering A, 2021, 810: 141021.
- [23] LI Lu, ZHANG Cun-cai, LV Hao, LIU Chun-rong, WEN Zhuo-zhang, JIANG Jing-wen. Texture development and tensile properties of Mg-Yb binary alloys during hot extrusion and subsequent annealing [J]. Journal of Magnesium and Alloys, 2022, 10: 249–265.
- [24] SOMEKAWA H, KINOSHITA A, KATO A. Great room temperature stretch formability of fine-grained Mg-Mn alloy [J]. Materials Science and Engineering A, 2017, 697: 217-223.
- [25] WANG Y N, HUANG J C. The role of twinning and untwinning in yielding behavior in hot-extruded Mg-Al-Zn alloy [J]. Acta Materialia, 2007, 55: 897-905.
- [26] HAN C S, GAO H J, HUANG Y G, NIX W D. Mechanism-based strain gradient crystal plasticity — I: Theory [J]. Journal of the Mechanics and Physics of Solids, 2005, 53: 1188–1203.
- [27] WU Xiao-lei, YANG Mu-xin, YUAN Fu-ping, CHEN Liu, ZHU Yun-tian. Combining gradient structure and TRIP effect to produce austenite stainless steel with high strength and ductility [J]. Acta Materialia, 2016, 112: 337–346.
- [28] MA Xiao-long, HUANG Chong-xiang, XU Wei-zong, ZHOU Hao, WU Xiao-lei, ZHU Yun-tian. Strain hardening and ductility in a coarse-grain/nanostructure laminate

- material [J]. Scripta Materialia, 2015, 103: 57-60.
- [29] ATEBA-BETANDA Y, HELBERT A L, BRISSET F, MATHON M H, WAECKERLÉ T, BAUDIN T. Measurement of stored energy in Fe-48%Ni alloys strongly cold-rolled using three approaches: Neutron diffraction, Dillamore and KAM approaches [J]. Materials Science and Engineering A, 2014, 614: 193-198.
- [30] KUBIN L P, MORTENSEN A. Geometrically necessary dislocations and strain-gradient plasticity: A few critical issues [J]. Scripta Materialia, 2003, 48: 119–125.
- [31] PAN Hu-cheng, KANG Rui, LI Jing-ren, XIE Hong-bo, ZENG Zhuo-ran, HUANG Qiu-yan, YANG Chang-lin, REN Yu-ping, QIN Gao-wu. Mechanistic investigation of a low-alloy Mg-Ca-based extrusion alloy with high strength ductility synergy [J]. Acta Materialia, 2020, 186: 278-290.
- [32] HONG S G, PARK S H, LEE C S. Role of {1012} twinning characteristics in the deformation behavior of a polycrystalline magnesium alloy [J]. Acta Materialia, 2010, 58: 5873–5885.
- [33] CHINO Y, KIMURA K, MABUCHI M. Twinning behavior and deformation mechanisms of extruded AZ31 Mg alloy [J]. Materials Science and Engineering A, 2008, 486: 481–488.
- [34] BARNETT M R, KESHAVARZ Z, BEER A G, ATWELL D L. Influence of grain size on the compressive deformation of wrought Mg-3Al-1Zn [J]. Acta Materialia, 2004, 52: 5093-5103.
- [35] SOMEKAWA H, BASHA D A, SINGH A. Deformation behavior at room temperature ranges of fine-grained Mg-Mn system alloys [J]. Materials Science and Engineering A, 2019, 766: 138384.
- [36] ANDO D, SUTOU Y, KOIKE J. Internal microstructure observation of enhanced grain-boundary sliding at room temperature in AZ31 magnesium alloy [J]. Materials Science and Engineering A, 2016, 666: 94–99.
- [37] SOMEKAWA H, BASHA D A, SINGH A. Room temperature grain boundary sliding behavior of fine-grained Mg-Mn alloys [J]. Materials Science and Engineering A, 2018, 730: 355-362.
- [38] ZENG Zhuo-ran, ZHOU Meng-ran, LYNCH P, MOMPIOU F, GU Qin-fen, ESMAILY M, YAN Yuan-ming, QIU Yao, XU Shi-wei, FUJII H, DAVIES C, NIE Jian-feng, BIRBILIS N. Deformation modes during room temperature tension of fine-grained pure magnesium [J]. Acta Materialia, 2021, 206: 116648.
- [39] ZHANG Yu-xiu, HUO Qing-huan, ZHANG Zhi-rou, XIAO Zhen-yu, HASHIMOTO A, YANG Xu-yue. Anisotropy in the tensile creep behaviors of hot-rolled Mg-5.5wt.%Y alloy sheet [J]. Materials Characterization, 2021, 172: 110843.
- [40] MALIK A, WANG Yang-wei, NAZEER F, KHAN M A, SAJID M, JAMAL S, WANG Ming-jun. Deformation behavior of Mg-Zn-Zr magnesium alloy on the basis of macro-texture and fine-grain size under tension and compression loading along various directions [J]. Journal of Alloys and Compounds, 2021, 858: 157740.
- [41] TONG Li-bo, ZHENG Ming-yi, XU Shi-wei, HU Xiao-shi, WU Kun, KAMADO S, WANG Guo-jun, LV Xin-yu. Room-temperature compressive deformation behavior of Mg-Zn-Ca alloy processed by equal channel angular pressing [J]. Materials Science and Engineering A, 2010, 528:

672-679.

- [42] ZHAO Lei, ZHANG Meng-na, WANG Jin-hui, SHI Bo, JIN Pei-peng. Effects of initial grain size and orientation on the twin behavior in ZK60 Mg alloy [J]. Materials Characterization, 2020, 167: 110496.
- [43] WEI Jian-sheng, YOU-jing, ZHANG Dong-dong, JIANG Shu-nong, CHEN Zhi-yong, LIU Chu-ming. Reducing yield asymmetry in a wrought Mg-9Al alloy by randomized texture achieved via multi-directional forging [J]. Materials Science and Engineering A, 2020, 796: 140003.
- [44] CHANG Li-li, WANG Yi-nong, ZHAO Xiang, QI Min. Grain size and texture effect on compression behavior of hot-extruded Mg-3Al-1Zn alloys at room temperature [J]. Materials Characterization, 2009, 60: 991–994.
- [45] TONG Li-bo, ZHENG Ming-yi, KAMADO S, ZHANG

- De-ping, MENG Jian, CHENG Li-ren, ZHANG Hong-jie. Reducing the tension-compression yield asymmetry of extruded Mg–Zn–Ca alloy via equal channel angular pressing [J]. Journal of Magnesium and Alloys, 2015, 3: 302–308.
- [46] HUPPMANN M, GALL S, MÜLLER S, REIMERS W. Changes of the texture and the mechanical properties of the extruded Mg alloy ME21 as a function of the process parameters [J]. Materials Science and Engineering A, 2010, 528: 342–354.
- [47] ZHAO Tian-shuo, HU Yao-bo, HE Bing, ZHANG Chao, ZHENG Tian-xu, PAN Fu-sheng. Effect of manganese on microstructure and properties of Mg-2Gd magnesium alloy [J]. Materials Science and Engineering A, 2019, 765: 138292.

热挤压和锻造制备高延性和高吸能 超细晶粒 Mg-Mn-Ce 合金

张宇修¹, 张至柔¹, 王春雨¹, 康宏辉¹, Hiromi NAGAUMI², 杨续跃¹

- 1. 中南大学 材料科学与工程学院,长沙 410083;
 - 2. 苏州大学 沙钢钢铁学院, 苏州 215100

摘 要:采用挤压和锻造低温变形方法制备高压缩延性和高吸能性超细晶粒 Mg-0.9Mn-0.5Ce (质量分数,%)合金。首先将合金在温度为 150 $\mathbb C$ 、挤压比为 12:1 的条件下进行挤压;随后,在 200 $\mathbb C$ 下沿挤压方向进行真应变为 1.2 的锻造处理。采用光学显微镜、扫描电镜、电子背散射衍射和透射电镜对合金的显微组织和塑性机理进行表征。结果表明,经低温挤压后合金组织由超细的动态再结晶晶粒和破碎的未再结晶晶粒组成,其平均晶粒尺寸为 1.9 μm。在随后的锻造过程中,逐渐产生新的超细晶粒,获得均匀的超细晶粒组织,其平均晶粒尺寸为 2.7 μm,织构强度也在锻造处理后减弱。均匀的超细晶粒组织和基面滑移使合金表现出较优的综合性能:压缩延性为 45.0%,吸能为 122.72 MJ/m³。

关键词: Mg-Mn-Ce 合金; 超细晶; 延性; 吸能

(Edited by Wei-ping CHEN)